

Comparing energy dissipation mechanisms within the vortex dynamics of gap and gapless nano-sized superconductors

E. C. S. Duarte,¹ E. Sardella,² T. T. Saraiva,³ A. S. Vasenko,^{3,4} and R. Zadorosny^{1,*}

¹*Superconductivity and Advanced Materials Group,
Departamento de Física e Química, Faculdade de Engenharia,
Univ Estadual Paulista–UNESP -Caixa Postal 31, 15385-000, Ilha Solteira, SP, Brazil.*

²*Superconductivity and Advanced Materials Group,
Faculdade de Ciências, Univ Estadual Paulista–UNESP,
Departamento de Física - Caixa Postal 473, 17033-360, Bauru, SP, Brazil*

³*HSE University, Moscow 101000, Russia*

⁴*I.E. Tamm Department of Theoretical Physics, P.N. Lebedev Physical Institute,
Russian Academy of Sciences, 119991 Moscow, Russia*

The presence of magnetic fields and/or transport currents can cause penetration of vortices in superconductors. Their motion leads to dissipation and resistive state arises, which in turn strongly affects the performance of superconducting devices such as single-photon and single-electron detectors. Therefore, an understanding of the dissipation mechanisms in mesoscopic superconductors is not only of fundamental value but also very important for further technological advances. In the present work, we analyzed the contributions and interplay of the dissipative mechanisms due to the locally induced electric field and an intrinsic relaxation of the superconducting order parameter, Ψ , in mesoscopic samples by using the time-dependent Ginzburg-Landau theory. Although often neglected, we show that the dissipated energy due to relaxation of Ψ must be taken into account for an adequate description of the total dissipated energy. The local increase of the temperature due to vortex motion and its diffusion in the sample were also analyzed, where the joint effect of thermal relaxation and vortex dynamics plays an important role for the dissipative properties presented by the superconducting systems.

I. INTRODUCTION

Mesoscopic superconductors present a variety of novel phenomena due to the confinement effects experienced by supercurrents and vortices. Such downsized materials have found applications in nanodevices like Superconducting Single-Photon Detectors (SSPDs) [1–9] and Superconducting Single-Electron Detectors (SSEDs) [10]. In both types of devices, a hot spot is created in the region where the particle (photon or electron) impacts the material and subsequently the heat diffuses through the material causing a local suppression of superconductivity. As a result, a spike of the measured voltage occurs caused by the burst of normal currents and the particle can thereby be detected [11]. It is therefore evident that the understanding of both the electrical and thermal properties of mesoscopic superconductors is very important in such and similar devices [12, 13].

When an external magnetic field is applied in a type II superconductor above the so-called “penetration field”, H_{c1} , magnetic flux in the form of Abrikosov vortices pierce the sample and the material transits into a mixed state [14, 15]. In the presence of electric current, the motion of those vortices dissipates energy, which results in a resistive state [16]. Several models have considered only the electric field induced by the moving vortices as a dissipation mechanism, which generates heat by the Joule effect [5, 17–19]. In this respect, Bardeen

and Stephen described the connection between the vortex velocity and the induced electric field by considering a viscous motion proportional to the square velocity of the vortex [20]. However, such a mechanism predicted much smaller damping than experimentally observed. Later on, Tinkham [21] proposed the existence of another dissipation mechanism, which is related to an intrinsic relaxation of the order parameter, Ψ . During the 90s and 2000s, the microscopic nature of the dissipative mechanisms and their influence on the viscosity and resistivity have been extensively studied experimentally up to recent years [22–25] with some experimental achievements [26, 27].

Despite that, there is still the need for more refined studies about how macroscopic parameters (within the time-dependent Ginzburg-Landau theory) affect the dissipation mechanism and, consequently, how they influence the thermal diffusion process. Also, due to the mesoscopic scale of these detectors, sample geometry plays a fundamental role yet not deeply addressed. By analyzing these issues, we present in this work a detailed mapping of the resistive state for nanoscale sizes square superconductors, with a focus on the thermal diffusion process during the Abrikosov’s vortex motion using the time-dependent Ginzburg-Landau formalism.

The next sections of this article are organized as follows: in Sec. II, we outline our theoretical methods applied in order to obtain our results. In Sec. III, we present our studies of the influence of the diffusion parameter, u , and the confinement effects on the resistive state for gap and gapless superconductors. In Sec. IV, we focus on

* rafazad@gmail.com

the behavior of the dissipative mechanisms, thermal diffusion and non-equilibrium aspects of the magnetization and voltage for both gap and gapless superconductors. In the last part, Sec. V we present the discussion of our results and the conclusions.

II. THEORETICAL FORMALISM

The time-dependent approach for the Ginzburg-Landau (TDGL) equations, which were firstly proposed by Schmid [28], provides a temporal evolution of the order parameter Ψ and the vector potential \mathbf{A} for a superconducting material submitted to an external applied magnetic field and/or a transport current for gapless superconductors. Later on, Kramer and Watts-Tobin presented a generalized version for the TDGL equations, which took into account the superconducting gap [29]. Both phenomenological non-equilibrium approaches are appropriate to describe most phenomena that occurs in the resistive state. The free energy theorem concerning the dissipative mechanism was first derived by Schmid [28]. In Reference [30], we generalized this theorem for gap superconductors. In some special circumstances, such theorem is in agreement with experimental observations, even for low temperatures [31]. Strictly speaking, both time dependent versions of the GL equations (either gapless or gap superconductors) are valid in the dirty limit and very close to T_c . Despite this limitation of Kramer-Watts-Tobin extension of the TDGL theory, some agreements with experiments can be achieved at temperatures as lower as $T = 0.5T_c$ [28, 31]. Those equations have also been applied in studies with induced voltage [32], magnetoresistance [17, 18], kinematic vortices [33], flux-flow regime [34, 35] and for samples under AC external magnetic fields [19]. The generalized time dependent Ginzburg-Landau (GTDGL) equations in dimensionless units are given by:

$$\frac{u}{\sqrt{1+\gamma^2|\Psi|^2}} \left(\frac{\partial}{\partial t} + i\varphi + \frac{1}{2}\gamma^2 \frac{\partial |\Psi|^2}{\partial t} \right) \Psi = (\nabla - i\mathbf{A})^2 \Psi + (1 - T - |\Psi|^2) \Psi \quad (1)$$

and

$$\left(\frac{\partial \mathbf{A}}{\partial t} + \nabla \varphi \right) = \mathbf{J}_s - \kappa^2 \nabla \times \nabla \times \mathbf{A}, \quad (2)$$

where the superconducting current density is

$$\mathbf{J}_s = \text{Im} [\Psi^* (\nabla - i\mathbf{A}) \Psi]. \quad (3)$$

Here, the order parameter is expressed in units of its bulk value at zero external field, $|\Psi_0|^2 = 8\pi^2 T_c^2 / 7\zeta(3)$, the distances are expressed in units of the coherence length at zero temperature $\xi(0)^2 = \frac{7\zeta(3)}{48\pi^2 T_c^2} \hbar^2 v_F^2$, where v_F is the Fermi velocity, and the magnetic field is expressed in units of the bulk upper critical field $H_{c2}(0) =$

$\Phi_0 / 2\pi\xi^2$, where $\Phi_0 = hc/2e$ is the quantum unit of flux. The temperature is expressed in units of T_c , time is in units of $t_{GL}(0) = \pi\hbar/8k_B T_c u$, the Ginzburg-Landau characteristic time; φ is the scalar potential and it is expressed in units of $V_0 = \hbar/2et_{GL}(0)$. The GL parameter is $\kappa = \lambda(0)/\xi(0)$, where $\lambda(0)$ is the London penetration depth at zero temperature. The parameter $\gamma = 2\Delta(0)\tau_{e-ph}/\hbar$ is related to the gap of the superconductor at zero temperature $\Delta(0) \approx 1.8k_B T_c$, where τ_{e-ph} is the electron-phonon inelastic collision time and k_B is the Boltzmann constant. The parameter u is given by the microscopic derivation of the Ginzburg-Landau equations. For a gapless superconductor, $\gamma = 0$, Gor'kov and Eliashberg obtained $u = 12$ [36]. In this case, Kramer and Baratoff [37] define $u = \frac{\tau_{|\Psi|}(0)}{t_{GL}(0)}$, with $\tau_{|\Psi|}(0)$ being the relaxation time of $|\Psi|$. On the other hand, for gap superconductors, $u = 5.79$ as demonstrated by Kramer and Watts-Tobin [29]. Several numerical algorithms have been developed to solve the TDGL equations numerically (see for instance References [38, 39]). We have used the link-variable method which ensures the gauge invariance when such equations are discretised on a numerical grid, as shown in [38]. For all times and positions we have chosen $\varphi = 0$, since neither charges nor external currents are considered in this work. To obtain the total dissipated power density, we generalized the Helmholtz free energy theorem proposed in the Reference [28] for a superconductor in an external magnetic field. Such equation, in dimensionless form, is given by:

$$W_{Total} = 2 \left(\left| \frac{\partial \mathbf{A}}{\partial t} \right| \right)^2 + \frac{2u}{\sqrt{1+\gamma^2|\Psi|^2}} \left[\left| \frac{\partial \Psi}{\partial t} \right|^2 + \frac{\gamma^2}{4} \left(\frac{\partial |\Psi|^2}{\partial t} \right)^2 \right]. \quad (4)$$

We distinguish the W_{Total} in the following dissipative mechanism:

$$W_{\mathbf{A}} = 2 \left(\left| \frac{\partial \mathbf{A}}{\partial t} \right| \right)^2, \quad (5)$$

$$W_{\Psi} = \frac{2u}{\sqrt{1+\gamma^2|\Psi|^2}} \left[\left| \frac{\partial \Psi}{\partial t} \right|^2 \right], \quad (6)$$

$$W_{\gamma} = \frac{2u}{\sqrt{1+\gamma^2|\Psi|^2}} \left[\frac{\gamma^2}{4} \left(\frac{\partial |\Psi|^2}{\partial t} \right)^2 \right]. \quad (7)$$

The extension of the Schmid theorem was first extended to the GTDGL equation in [30].

The first term is the dissipation due to the induced electric field, $W_{\mathbf{A}}$, the second one is related to the relaxation of the order parameter, W_{Ψ} , and the last term is due to the relaxation of the density of superelectrons, W_{γ} . The dissipated power density is given in units of $(a_0 T_c)^2 / bt_{GL}(0)$, where a_0 and b are the phenomenological GL parameters [40]. As the dissipated energy diffuses

through the sample, we coupled the thermal diffusion equation to the GTDGL ones. By using the approach of Ref. [32], the dimensionless form of the thermal equation takes the form:

$$C'_{eff} \frac{\partial T}{\partial t} = K_{eff} \nabla^2 T + \frac{1}{2} W_{Total} - \eta(T - T_0), \quad (8)$$

where η is the heat-transfer coefficient to the substrate, T_0 is the bath temperature, $C'_{eff} = \pi^4/48u$ is the effective heat capacity, and $K_{eff} = \pi^4/48u^2$ is the effective thermal conductivity. As one can see, the parameter u influences the behavior of the thermal properties as well.

To minimize the time spent by the simulations, several works used $u \leq 1$ without losing qualitative correspondence to experimental data [17, 41]. However, the right values of u must be used in studies of non-equilibrium processes such as thermal dissipation and diffusion. To have a proper correspondence to experimental data, the GTDGL equations must follow the condition $1 - T < \frac{u^{1/2}}{\gamma}$ [42]. On the other hand, for $\gamma = 0$, we recover the TDGL equations, which are derived for the case of a large a concentration of paramagnetic impurities, i.e., $u = 12$ and $T \rightarrow T_c$ or $(H \rightarrow H_{c2})$ [43]. References [44–46] report such modifications to properly describe the gapless superconductors.

III. INFLUENCE OF THE DIFFUSION PARAMETER u OVER THE DISSIPATION RESISTIVE STATE

We carried out numerical simulations for square thin films with lateral sizes ranging from $L = 10\xi(0)$ to $100\xi(0)$, such as sketched in Fig. 1. We employed the superconductor/insulator boundary condition, i.e. the normal component of the superconducting current at the boundary is zero: $\mathbf{n} \cdot (\nabla - i\mathbf{A})\Psi = 0$, and also we assumed that all the heat is transferred to the substrate, which means $\mathbf{n} \cdot (\nabla T) = 0$. In all cases, the mesh was set as $\Delta x = \Delta y = 0.1\xi(0)$, the GL parameter $\kappa = 5$ and the bath temperature $T_0 = 0.93T_c$. The external magnetic field was varied in steps of $\Delta H = 10^{-3}H_{c2}(0)$ and the heat-transfer coefficient η was set as 2×10^{-4} . This is an intermediate value for heat removal as discussed in Reference [32]. The density of power dissipation was analyzed during the first vortex penetration by setting the diffusion parameter u equal to 1, 5.79 and 12.

The evolution of the spatial averages of the contributions to dissipation, $\langle W_{\mathbf{A}} \rangle$ and $\langle W_{\Psi} \rangle$, is shown in Fig. 2 for samples with sides $L = 60\xi(0)$ and $L = 80\xi(0)$ for $u = \{1, 5.79, 12\}$. As one can notice, increasing the parameter u does not influence the qualitative behavior of the system, but can decrease the dissipation around one order of magnitude. Also, the total duration of the event is longer for the largest sample, $L = 80\xi(0)$. Besides that, the maximum of the dissipation is reached faster for smaller sample. Such behavior occurs when

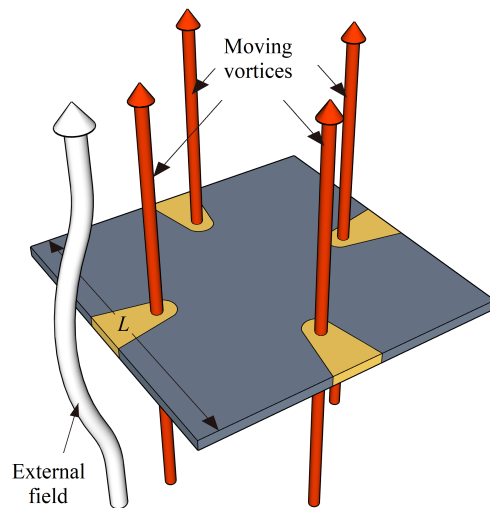


FIG. 1. Sketch of the square superconducting thin film submitted to a perpendicular external magnetic field. Here we show the moment when four quantum of fluxes penetrate the sample dissipating heat and causing a local increase in temperature, represented by the yellow region.

the lateral size of the sample is near to the meso-macro crossover according to the criterion used in Ref. [47].

In Fig. 3 it is shown the maximum values reached by $W_{\mathbf{A}}$, W_{Ψ} and $W_{total} = W_{\mathbf{A}} + W_{\Psi}$ as functions of the lateral size of the samples, for the first vortex penetration. We can observe that all dissipative mechanisms increase for $L \geq 40\xi(0)$, where the first penetration corresponds to four or more vortices. For such values of L , the vortices have more space to move freely before their repulsive interaction becomes more pronounced. Such a fact explains the increasing dissipation for larger values of L . On the other hand, confinement effects for $L = 20\xi(0)$ are responsible for the penetration of only two vortices. Then, the repulsive interaction is present since the beginning of their penetration (see Reference [47]). Besides that, the shielding current produces a greater Lorentz force over the two penetrated vortices making their dissipation larger in comparison with $L = 40\xi(0)$. From Fig. 3(d) we can also notice a saturation tendency of the dissipative mechanisms curves when the transition from the mesoscopic to the macroscopic regime is reached, which occurs around $L = 80\xi(0)$ for $T_0 = 0.93T_c$. It is remarkable that this value is very closed to the one predicted in Ref. [47]. Furthermore, in Fig. 2(d) it was obtained $W_{total}^{u=5.79} \simeq W_{total}^{u=12}$ with $20\xi(0) \leq L \leq 40\xi(0)$. As we pointed out in Sec. II, those cases were derived from similar approaches for both values of u , i.e., derived considering the dirty limit of a microscopic theory. This result corroborates the consistency of our models with the microscopic theory. In short, for small superconducting systems, where strong confinement effects drive the vortex dynamics, there is no physical difference in describing those systems by using either $u = 12$ or $u = 5.79$ when

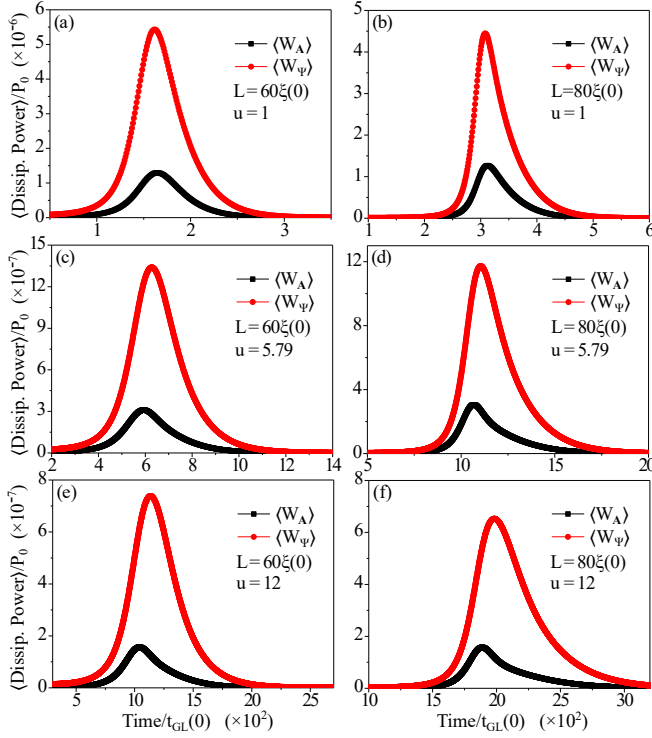


FIG. 2. Average dissipated power density as a function of time during the first vortex penetration for samples with dimensions $L = 60\xi(0)$ (left column) and $L = 80\xi(0)$ (right column) for some values of u and $T_0 = 0.93T_c$.

the dissipated power is taken into account.

Concluding this section, we analyzed the influence of u over the magnetization and the voltage pulse induced by the first flux penetration (see Fig. 4). One can notice that the characteristic time of the whole event grows almost linearly with u when expressed in units of t_{GL} . We obtained characteristic times around $350t_{GL}(0)$, $1200t_{GL}(0)$ and $2500t_{GL}(0)$ for $u = 1, 5.79, 12$, respectively. But, in general, one can express these time values in seconds as $t_{GL} \approx 3 \times 10^{-12}/T_c u$. Using the parameters for WSi from Ref. [48], $T_c = 3.5K$, this means that the characteristic times for this penetration of vortices happen within $\sim 300ps$ (with $u = 1$), $\sim 178ps$ (with $u = 5.79$) and $\sim 179ps$ (with $u = 12$). We believe that u should be high for amorphous samples. The amplitude of the voltage pulse decreases with u when expressed in units of V_0 : $5.5 \times 10^{-2}V_0$, $1.5 \times 10^{-2}V_0$ and $0.88 \times 10^{-2}V_0$ for $u = 1, 5.79, 12$. Again, we can consider the case of WSi and get the modulus of these voltage peaks between $\sim 7.7 \times 10^{-8}statV$ for $u = 1$, $\sim 1.2 \times 10^{-7}statV$ for $u = 5.79$ and $\sim 1.5 \times 10^{-5}statV$ for $u = 12$.

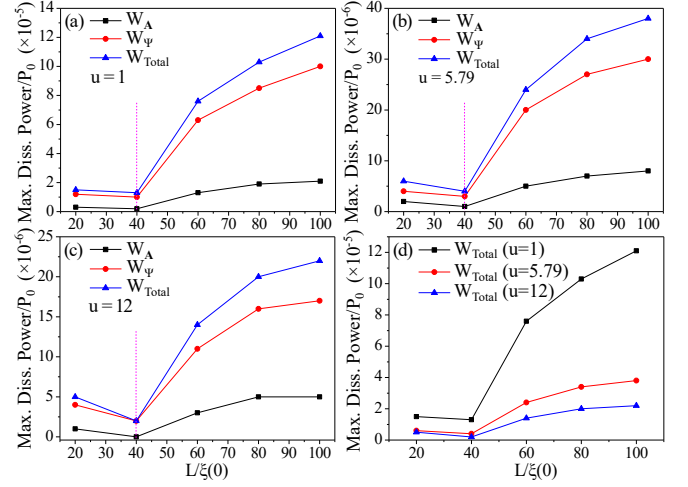


FIG. 3. Local maximum of the dissipated power density for different values of u as a function of lateral size L at $T_0 = 0.93T_c$. The dashed line indicates a vorticity transition from 2 to 4 vortices.

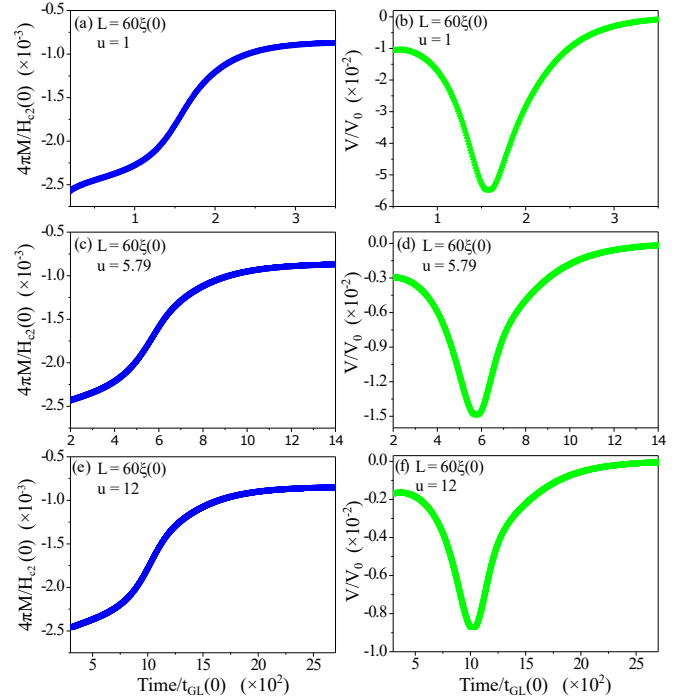


FIG. 4. Magnetization (left column) and voltage (right column) as functions of time during the vortex penetration for different values of u .

IV. RESISTIVE STATE OF VORTEX-MOTION IN A MULTIPLY-CONNECTED SAMPLE

In order to study the dissipative mechanisms during the motion of a single-vortex in detail, we simulated square superconducting samples with size L and a central square hole (or antidot, AD), with side w .

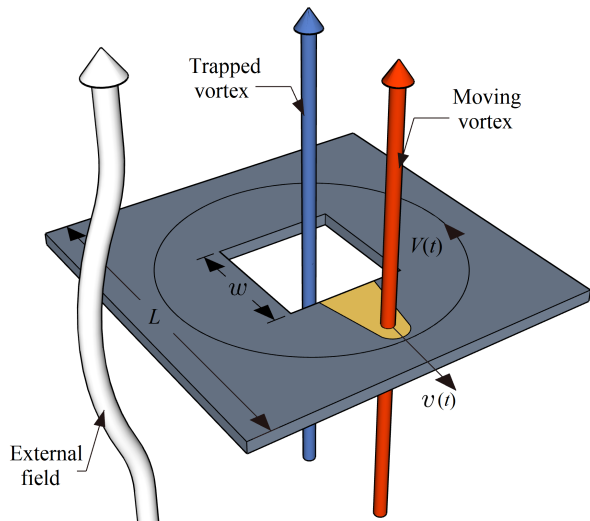


FIG. 5. Sketch of the thin square superconducting film with an square occlusion in the center with side w . After trapping two vortices in the sample, one can decrease the external field (represented by a white arrow) and one of the fluxes leave the sample with velocity v and creating a “hotspot”. The blue arrow represents the trapped vortex that remains in the sample and the red one represents the flux quantum that leaves the sample. During this process, a non-zero voltage, $V(t)$, around the sample can be measured.

The applied magnetic field was increased in steps of $\Delta H = 10^{-3}H_{c2}(0)$ up to the penetration of two vortices and their consequent trapping in the AD. After that, the applied magnetic field was decreased until the depinning of one vortex, as sketched in Fig. 5.

A. Gapless superconductors

The process of a quantum flux leaving the sample has many aspects to be investigated. For example, the current induced by the spike in the voltage has to flow partly through the center of the vortex, which is a normal state region and this causes dissipation. In Fig. 6, it is shown the local maxima of $W_{\mathbf{A}}$, W_{Ψ} , and W_{total} as functions of the vortex velocity when moving out of the sample, v . In order to investigate how the relation between the dissipative mechanisms and the vortex velocity depends on the geometry, we fixed the dimension of the square $L = 26\xi(0)$ and considered two different values of the AD size, w . On the left-hand side of Fig. 6 one finds the data for $w = 4\xi(0)$ and on the right-hand side for $w = 6\xi(0)$. In general, one can see that the dissipated power increase monotonically as functions v , as expected. But the system with $w = 6\xi(0)$ shows smaller values for both W_{Ψ} and $W_{\mathbf{A}}$ which is related to the fact that the vortex is concentrated in a smaller region for $w = 4\xi(0)$. To understand such behavior, we plotted the intensity of $|\Psi|$ for those values of w with $L = 26\xi(0)$, as illustrated in

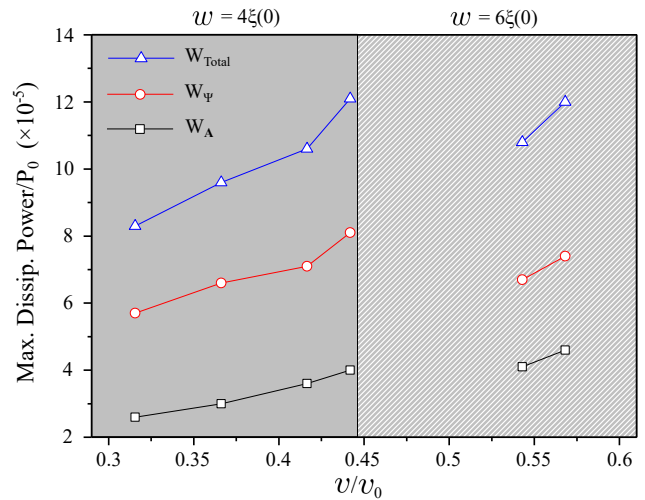


FIG. 6. Relation between the local maximum of the dissipated power and the vortex velocity, v , for a gapless superconductor (i.e. $\gamma = 0$) at $T = 0.93T_c$. The gray region contains the results for the sample with $w = 4\xi(0)$ while the dashed stands for $w = 6\xi(0)$.

the panels of Fig. 7. They show that the vortex core becomes more stretched in the y direction as the velocity of the vortex increases, by forming a phase-slip-like region, similar to a *vortex street* [49]. This change in the vortex core shape affects the time-variation of $|\Psi|$ (see the plots in Fig. 7). It can be seen that the maximum value of $\Delta|\Psi|$ is lower for the sample with $w = 6\xi(0)$ and consequently W_{Ψ} decreases. Also, these panels show that the modulus of the order parameter increases sharply after the vortex core in the direction to the boundary while it is slowly increasing in the direction to the hole in the center of the sample. In other words, the second derivative of the modulus of order parameter changes sign after crossing the vortex core.

As expected, vortex motion is accompanied by dissipation of heat and a local increase of the temperature. In Fig. 8, it is shown snapshots of the intensity of each dissipative mechanisms, and the variation of the local temperature, $\Delta T = T - T_0$, when the vortex is about to leave the sample. We chose the moment when W_{Total} reaches its local maximum (also seen in Fig. 6 that it is the moment of fastest vortex velocity). The maximum dissipated power W_{Ψ} shows around one order of magnitude larger than $W_{\mathbf{A}}$ being the main responsible for the local increase in temperature. One can see in Fig. 8 that ΔT follows directly the behavior of W_{Total} , i.e. it is larger when the vortex is about to leave at the lower edge of the sample and its velocity is maximum. Furthermore, in these plots shown in Fig. 8, the dissipation shows a particular behavior near the outer edges of the sample for each contribution. The term $W_{\mathbf{A}}$ is more pronounced near the edges of the sample [50], while W_{Ψ} shows less influence by shading from the corners. This can be inter-

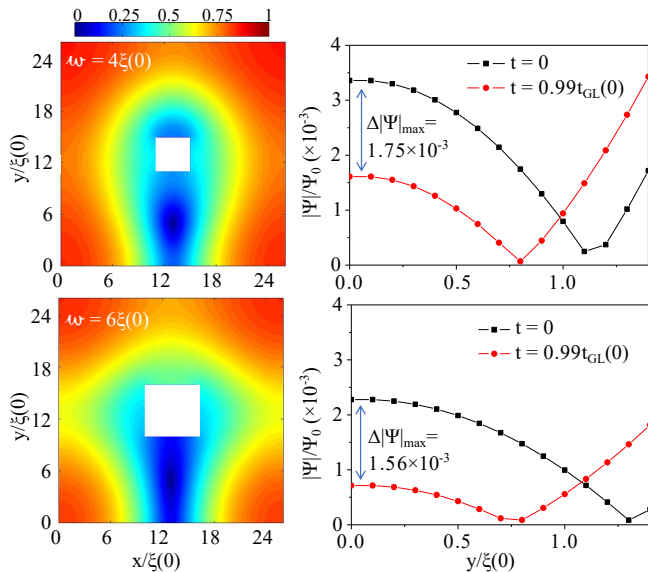


FIG. 7. On the left, the intensity of $|\Psi|$ illustrates the changing on the vortex shape for two samples of size $L = 26\xi(0)$, for $w = 4\xi(0)$ (upper left panel) and $w = 6\xi(0)$ (lower left panel). In both panels the core of the vortex is localized at $y = 5.0\xi(0)$. The right panels show the variations of $|\Psi|$ along the vortex core just before the vortex leaves the sample in a time interval defined from $t = 0$ to $t = 0.99t_{GL}(0)$ along the vertical line $x = 13\xi(0)$, i.e. the middle of the sample.

preted by the fact that the superconducting currents can better circulate near the corners while not so much near the edges and thus the stronger effect over $W_{\mathbf{A}}$. This influence from the corners affects the total dissipation but becomes slightly less visible in the temperature change ΔT .

B. Gap superconductor

We also studied the dissipative mechanisms during the vortex motion in a gap superconductor, i.e. we considered $\gamma \neq 0$ in Eq. (1). For the sake of estimating its order of magnitude, one can use the BCS expression for the gap $\Delta(0) = 1.76k_B T_c$ and substitute in the definition shown in the Sec. II, $\gamma = 2\Delta(0)\tau_{e-ph}/\hbar$. Furthermore, based on the values obtained for WSi in Ref's. [48, 51, 52], ranging from 75ps to 190ps, i.e. within the order $\tau_{e-ph} \sim 10^{-10}$ s with $T_c \sim 10^0 K$. This means that $\gamma \sim 10^1$.

The setup of the simulation and shape of the samples were similar to the ones considered previously in Sec. IV A, i.e. thin square films with a square hole in the center, and the magnetic field was decreased until a vortex moves out of the sample. Along the whole set of parameters that we covered (γ , L , w), the extra dissipated power due to this term, $\langle W_\gamma \rangle$, was typically smaller or of the same order of magnitude than the other contributions, $\langle W_{\mathbf{A}} \rangle$ and $\langle W_{\Psi} \rangle$, as shown in Fig. 9 for $L = 26\xi(0)$,

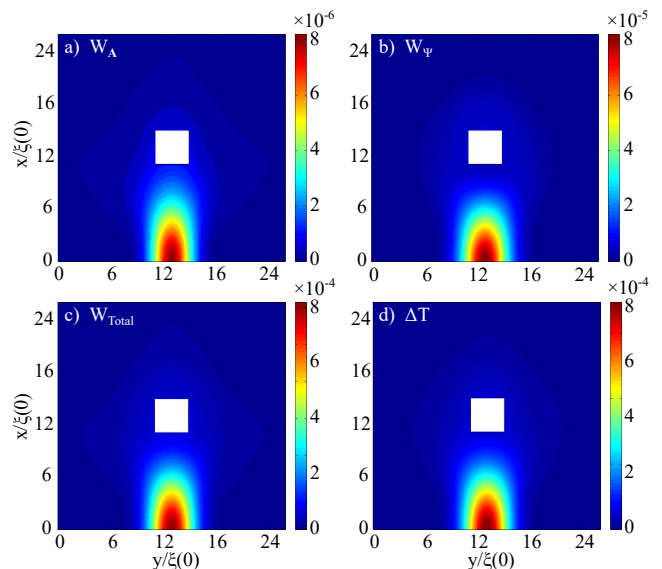


FIG. 8. Local intensity profile of the dissipated power functions and the local variation of temperatures for a gapless superconductor ($\gamma = 0$) with parameters $L = 26\xi(0)$ with $w = 4\xi(0)$. The snapshot corresponds to the moment where one of the two trapped vortices is about to leave the sample. This is the moment of maximum dissipation and also the point of highest vortex velocity.

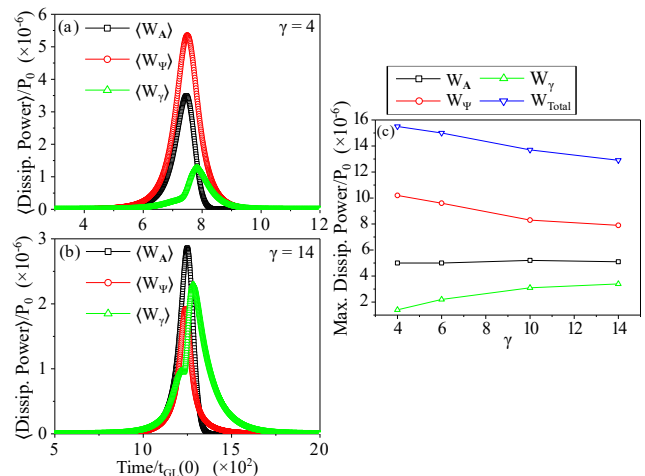


FIG. 9. Average dissipated power density as a function of time for (a) $\gamma = 4$ and (b) $\gamma = 14$. In (c) it is shown the local maximum of the dissipated power density as a function of γ .

$w = 4\xi(0)$, and $u = 5.79$. One can see in panels (a) and (b) that $\langle W_\gamma \rangle$ increases with γ , whereas $\langle W_\Psi \rangle$ decreases. It is interesting to note that this is a direct consequence of their dependence on γ in Eq's. 7 and 6. Also, as expected, $\langle W_{\mathbf{A}} \rangle$ is practically not affected, also expected from the definition in Eq. 5. The total dissipation decreases with γ , indicating that the dissipation is stronger

in gap superconductors for this particular setup. In addition, the local maximum power dissipation in panel 9-(c) shows that this trend maintains or, in other words, W_Ψ decreases while W_γ increases smoothly and the maximum of W_{total} decreases smoothly with increasing γ as well.

In Fig. 10 we present snapshots of the three dissipative mechanisms and their sum, W_{total} , and ΔT for $\gamma = 4$ and $\gamma = 14$. Following the trend discussed about Fig. 9, one sees that W_Ψ is decreased with γ while W_A increases. In addition, the shading effect over W_A is also noticeable and less present in the other terms, similar to the gapless system. One can also notice that ΔT also is less pronounced next to the corners and it is clearly greater for $\gamma = 4$ than for $\gamma = 14$.

By analyzing the local maximum dissipated power as a function of the vortex velocity for $\gamma = 4$, shown in Fig. 11-(a), it can be seen that W_A and W_Ψ increase with the velocity, while W_γ stays nearly constant. Besides, the vortex velocity decreases with γ , as seen in Fig. 11(b), which can be explained roughly by the presence of γ in the denominator multiplying the time-derivative in Eq. 1. In fact, this means an increase in the effective viscosity with γ .

Continuing the study of gap systems, we plotted the time-evolution of both magnetization $M(t)$ and induced voltage $V(t)$ during the vortex motion. The influence of γ is qualitatively small, as shown in Fig. 12, with only a slight change in the amplitude of the curves. The magnetization of the sample starts from a negative value and ends in a smaller value in modulus after the vortex leaves the sample. This whole process can be easily understood under the scope of the Ampère law, where essentially a variation of the magnetic flux over the sample is related to a voltage around it. The series of 6 points selected along the curves starts with the vortex leaving the occlusion in the center and piercing the film, (a), until the vortex leaving the sample, (f). These snapshots are shown in Fig. 13. The local voltage maximum occurs in instants just before a vortex leaves the sample, seen in Figure 13-(c). In opposition, the maximum magnetization occurs for the vortex leaving the sample (close to $V(t) = 0$), as it is shown in Fig. 13-(d). Also, a negative voltage peak indicates a recovering of the superconducting state or, in other words, an increasing of the modulus of the order parameter in the lower edge of the sample after the vortex leaves the sample, seen in the sequence from 13-(d) to (f).

V. DISCUSSION OF THE RESULTS AND CONCLUSIONS

Our study of the resistive state in a gapless superconductor shows that the dissipative mechanisms and the induced voltage are u -dependent. Concerning such an issue, Vodolazov and Peeters previously verified that u plays an important role, but solely on the relaxation of Ψ [41]. Nonetheless, the magnetization does not

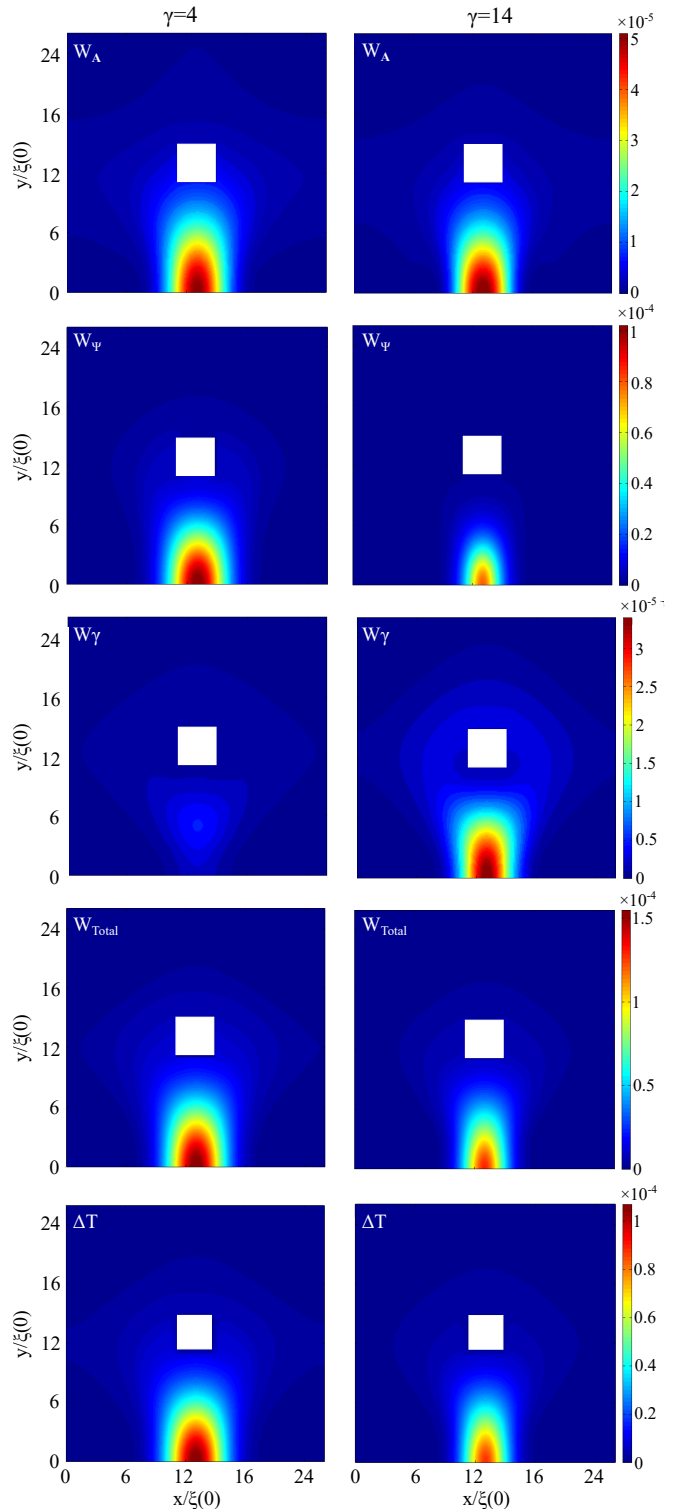


FIG. 10. Plots of the the local dissipative mechanisms, W_A , W_Ψ , W_γ , W_{total} and the local variation of temperature, ΔT , for $\gamma = 4$ (left column) and $\gamma = 14$ (right column). The snapshots were taken from the moment when the vortex is about to leave the sample.

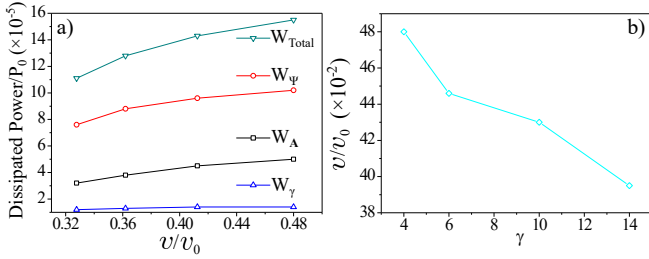


FIG. 11. (a) The three dissipative mechanisms and their sum, W_{total} , as a function of the vortex velocity for $\gamma = 4$; (b) vortex velocity (taken just before it left the sample) as function of γ for the sample $L = 26\xi(0)$ and $w = 4\xi(0)$.

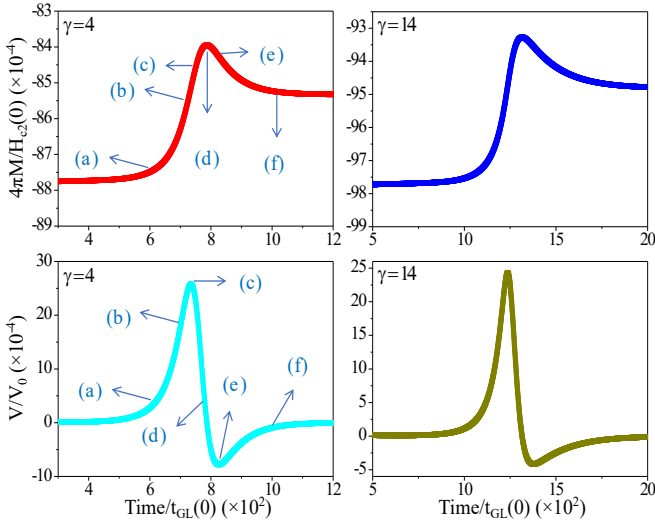


FIG. 12. Magnetization and voltage as function of the time during the process of one vortex leaving the sample for $\gamma = 4$ (left column) and $\gamma = 14$ (right column).

present a considerable variation by changing u . For the clean limit (or with small paramagnetic impurities, i.e., $u = 5.79$), the superconducting systems present significant differences between W_{Λ} , W_{Ψ} , and V for all sizes of the studied samples. Furthermore, it was showed that for $20\xi(0) \leq L \leq 40\xi(0)$, W_{total} is nearly the same for both $u = 5.79$ and $u = 12$.

Except W_{γ} , all the other dissipative mechanisms are sensitive to the vortex velocity for both gap and gapless superconductors. W_{Ψ} and W_{γ} presented significant variations with γ as well as the shape of the vortex core. In Fig. 14, W_{total} and ΔT were compared for both gapless and gap systems by considering a sample with $L = 26\xi(0)$, and $w = 4\xi(0)$ at $T_0 = 0.93T_c$. Despite W_{total} in a gap sample being greater than in a gapless one, ΔT is higher for gapless superconductors. Such a fact is due to the u -dependence of C_{eff} and K_{eff} . Then, in the numerical solution of the TDGL equations coupled with the diffusion equation, ΔT increases proportionally with u . In addition, it is worth

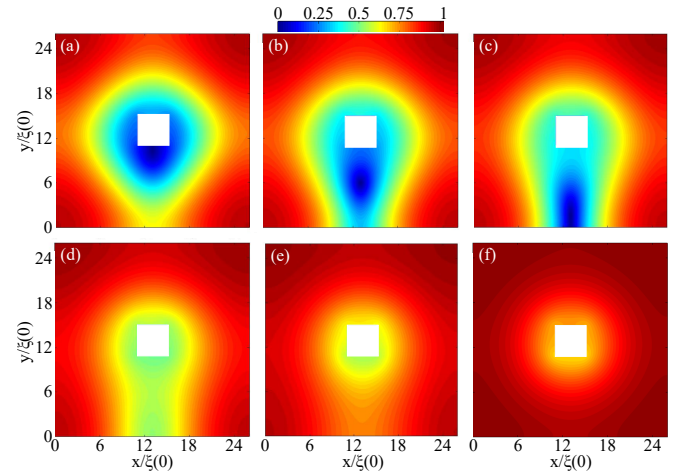


FIG. 13. Snapshots of $|\Psi|$ exhibiting the vortex dynamics for $\gamma = 4$ at instants (a) to (f) indicated in Figure 12.

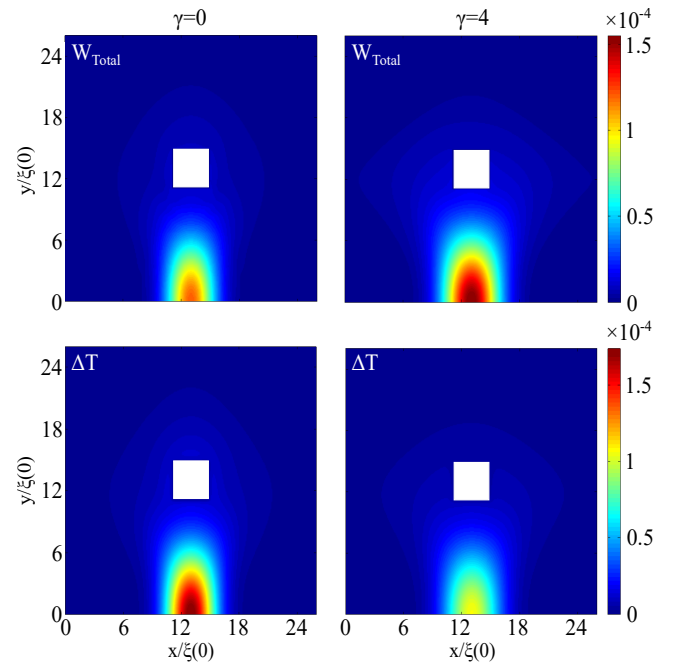


FIG. 14. Comparing W_{total} and ΔT between a gap ($\gamma = 4$) and a gapless ($\gamma = 0$) superconductor for $L = 26\xi(0)$ and $w = 4\xi(0)$.

noticing that in our simulations for $\gamma = 4, 6, 10$, and 14 we obtained $\Delta T_{\text{gap}} > \Delta T_{\text{gapless}}$ and $W_{\text{total}}^{\text{gap}}/W_{\text{total}}^{\text{gapless}} \approx u_{\text{gapless}}/u_{\text{gap}} = 12/5.79 = 2.07$.

It was shown that W_{Ψ} governs the dissipation of Abrikosov vortex dynamics, and it is of fundamental importance for the evaluation of ΔT . Besides, other theoretical works showed that W_{total} depends on the Ψ relaxation for $H \ll H_{c2}$ [43, 53]. Kupriyanov and Likharev demonstrated that $\frac{\Gamma_R}{\Gamma_N} = 1.7547$, is the rate between the normal electron relaxation time (Γ_N) and the Ψ relaxation time for gapless superconductors (Γ_R). Considering

Γ_N related to W_Ψ and Γ_R related to W_A , one obtained $1.61 < \frac{W_\Psi}{W_A} < 2.19$ (from Figure 5), which is in accordance with [53]. On the other hand, for the gap systems ($\gamma = 4$) the ratio $2.04 < \frac{W_\Psi}{W_A} < 2.37$ (from Figure 8) and therefore, our results agree with Ref. [53], i.e. W_A is essentially not affected by γ while W_Ψ increases. As found in the literature, resistivity is related to the dissipated power during vortex motion. However, just a few works compare experimental results with the theoretical ones at $H \ll H_{c2}$. In the works of Fogel [54], and Gubankov *et al.* [55], it was shown that the viscosity is lower than that one verified experimentally by considering dissipation just caused by normal electrons.

However, by taking into account the power dissipation due to relaxation of Ψ , an excellent experimental agreement is reached [54]. For a thin film with a small concentration of paramagnetic impurities, the process involving the relaxation of Ψ is also the main dissipative mechanism [56]. Poon and Wong showed that, by measuring the electrical properties of Zr_3Ni and Zr_3Rh bulk samples, it is not possible to obtain an experimental agreement by considering just one type of dissipative mechanism. Nonetheless, when all dissipative mechanisms are considered, it is possible to obtain an excellent agreement with experimental data. Therefore, the contributions of the relaxation terms and the normal currents are of great importance and agree well with experiments in the temperature range $0.66T_c < T_0 < 0.95T_c$ [57]. It is important to emphasize that the experimental data in previous studies [54, 56, 57], agreed well with those ones from theoretical works [20, 21, 43, 53], where the dissipative mechanisms were obtained in a different formalism than we presented here. In this work, all dissipative mechanisms were de-

rived from the generalization of the free energy theorem [28, 30]. Thus, all dissipative mechanisms that are experimentally relevant for an accurate description of metallic superconducting materials were considered. It is worth mentioning that the values obtained for ΔT are of the order of $10^{-4}T_c$ and are suitable to be measured with nanoSQUIDs as it was demonstrated by Halbertal *et al.* [58]. For the $H \ll H_{c2}$ regime, one demonstrated that W_Ψ is of great importance to W_{total} , and consequently to ΔT . Furthermore, the vortex velocity and the nanostructured superconductors geometry influence the values of W_Ψ . For gap superconductors, it was shown that lower γ (≤ 4) increases W_Ψ .

In conclusion, our theoretical approach aims to describe dissipative and thermal diffusion processes in superconducting devices such as single-photon detectors, fluxonic cellular automata [59, 60], or vortex random access memory [61], where the control of the dissipation during vortex motion is very important to reach a reliable performance. The characteristic times obtained for vortex motion are in accordance with experimental results for the characteristic times

We acknowledge the support from the Brazilian agencies: São Paulo Research Foundation, FAPESP, grants 2016/12390-6 and 2020/10058-0, Coordenação de Aperfeiçoamento de Pessoal de Nível Superior - Brasil (CAPES) - Finance Code 001, and National Council of Scientific and Technological Development (CNPq, grant 310428/2021-1) for financial support. The work at HSE University (T.T.S. and A.S.V.) was supported by the framework of the Academic Fund Program at HSE University in 2021 (Grant No. 21-04-041).

-
- [1] G N Gol'tsman, O Okunev, G Chulkova, A Lipatov, A Semenov, K Smirnov, B Voronov, A Dzardanov, C Williams, and R Sobolewski. Picosecond superconducting single-photon optical detector. *Applied physics letters*, 79(6):705–707, 2001.
- [2] A J Kerman, E A Dauler, J K W Yang, Kristine M Rosfjord, V Anant, K K Berggren, G N Gol'tsman, and B M Voronov. Constriction-limited detection efficiency of superconducting nanowire single-photon detectors. *Applied Physics Letters*, 90(10):101110, 2007.
- [3] S N Dorenbos, E M Reiger, U Perinetti, V Zwiller, T Zijlstra, and T M Klapwijk. Low noise superconducting single photon detectors on silicon. *Applied Physics Letters*, 93(13):131101, 2008.
- [4] Robert H. Hadfield. Single-photon detectors for optical quantum information applications. *Nature Photonics*, 3(12):696–705, Dec 2009.
- [5] G R Berdiyrov, M V Milošević, and F M Peeters. Spatially dependent sensitivity of superconducting meanders as single-photon detectors. *Applied Physics Letters*, 100(26):262603, 2012.
- [6] A N Zotova and D Yu Vodolazov. Photon detection by current-carrying superconducting film: A time-dependent ginzburg-landau approach. *Physical Review B*, 85(2):024509, 2012.
- [7] Chandra M Natarajan, Michael G Tanner, and Robert H Hadfield. Superconducting nanowire single-photon detectors: physics and applications. *Superconductor Science and Technology*, 25(6):063001, apr 2012.
- [8] R Gaudio, K P M Op't Hoog, Z Zhou, D Sahin, and A Fiore. Inhomogeneous critical current in nanowire superconducting single-photon detectors. *Applied Physics Letters*, 105(22):222602, 2014.
- [9] J J Renema, R J Rengelink, I Komen, Q Wang, R Gaudio, K P M op't Hoog, Z Zhou, D Sahin, A Fiore, P Kes, et al. The effect of magnetic field on the intrinsic detection efficiency of superconducting single-photon detectors. *Applied Physics Letters*, 106(9):092602, 2015.
- [10] M Rosticher, F R Ladan, J P Maneval, S N Dorenbos, T Zijlstra, T M Klapwijk, V Zwiller, A Lupaşcu, and G Nogues. A high efficiency superconducting nanowire single electron detector. *Applied Physics Letters*, 97(18):183106, 2010.
- [11] Alexei D Semenov, Gregory N Gol tsman, and Roman Sobolewski. 15(4):R1–R16, mar 2002.
- [12] A. G. Kozorezov, A. F. Volkov, J. K. Wigmore, A. Pea-

- cock, A. Poelaert, and R. den Hartog. Quasiparticle-phonon downconversion in nonequilibrium superconductors. *Phys. Rev. B*, 61:11807–11819, May 2000.
- [13] J K W Yang, A J Kerman, E A Dauler, V Anant, K M Rosfjord, and K K Berggren. Modeling the electrical and thermal response of superconducting nanowire single-photon detectors. *IEEE transactions on applied superconductivity*, 17(2):581–585, 2007.
- [14] A. A. Abrikosov. On the magnetic properties of superconductors of the second group. *J. Exptl. Theoret. Phys.*, 32:1174–1182, 1957.
- [15] E H Brandt. The flux-line lattice in superconductors. *Reports on Progress in Physics*, 58(11):1465–1594, nov 1995.
- [16] Michael Tinkham. *Introduction to superconductivity*. McGraw-Hill New York, 1975.
- [17] G R Berdiyrov, X H Chao, F M Peeters, H B Wang, V V Moshchalkov, and B Y Zhu. Magnetoresistance oscillations in superconducting strips: a ginzburg-landau study. *Physical Review B*, 86(22):224504, 2012.
- [18] G R Berdiyrov, M V Milošević, M L Latimer, Z L Xiao, W K Kwok, and F M Peeters. Large magnetoresistance oscillations in mesoscopic superconductors due to current-excited moving vortices. *Physical review letters*, 109(5):057004, 2012.
- [19] A D Hernández and D Domínguez. Dissipation spots generated by vortex nucleation points in mesoscopic superconductors driven by microwave magnetic fields. *Physical Review B*, 77(22):224505, 2008.
- [20] J Bardeen and M J Stephen. Theory of the motion of vortices in superconductors. *Physical Review*, 140(4A):A1197, 1965.
- [21] M Tinkham. Viscous flow of flux in type-II superconductors. *Physical Review Letters*, 13(26):804, 1964.
- [22] E.M. Gershenzon, M.E. Gershenzon, G.N. Gol’tsman, A.D. Semyonov, and A.V. Sergeev. Heating of electrons in superconductor in the resistive state due to electromagnetic radiation. *Solid State Communications*, 50(3):207–212, 1984.
- [23] E.M. Gershenzon, G.N. Gol’tsman, A.D. Semenov, and A.V. Sergeev. Mechanism of picosecond response of granular ybaco films to electromagnetic radiation. *Solid State Communications*, 76(4):493–497, 1990.
- [24] F. Marsili, M. J. Stevens, A. Kozorezov, V. B. Verma, Colin Lambert, J. A. Stern, R. D. Horansky, S. Dyer, S. Duff, D. P. Pappas, A. E. Lita, M. D. Shaw, R. P. Mirin, and S. W. Nam. Hotspot relaxation dynamics in a current-carrying superconductor. *Phys. Rev. B*, 93:094518, Mar 2016.
- [25] Ahmad Sheikhzada and Alex Gurevich. Dynamic pair-breaking current, critical superfluid velocity, and nonlinear electromagnetic response of nonequilibrium superconductors. *Phys. Rev. B*, 102:104507, Sep 2020.
- [26] Ken’ichi Tanaka, Yoshiro Arikawa, Matsuo Sekine, Motoichi Ohtsu, Yuichi Harada, and Martin Danerud. Highly sensitive and wideband optical detection in patterned $\text{YBa}_2\text{Cu}_3\text{O}_{7-\delta}$ thin films. *Applied Physics Letters*, 68(22):3174–3176, 1996.
- [27] David Bitauld, Francesco Marsili, Alessandro Gaggero, Francesco Mattioli, Roberto Leoni, Saeedeh Jahanmiri Nejad, Francis Lévy, and Andrea Fiore. Nanoscale optical detector with single-photon and multiphoton sensitivity. *Nano Letters*, 10(8):2977–2981, Aug 2010.
- [28] A Schmid. A time dependent ginzburg-landau equation and its application to the problem of resistivity in the mixed state. *Physik der kondensierten Materie*, 5(4):302–317, 1966.
- [29] L Kramer and R J Watts-Tobin. Theory of dissipative current-carrying states in superconducting filaments. *Physical Review Letters*, 40(15):1041, 1978.
- [30] ECS Duarte, E Sardella, WA Ortiz, and R Zadorosny. Dynamics and heat diffusion of abrikosov’s vortex-antivortex pairs during an annihilation process. *Journal of Physics: Condensed Matter*, 29(40):405605, 2017.
- [31] I Petković, A Lollo, L I Glazman, and J G E Harris. Deterministic phase slips in mesoscopic superconducting rings. *Nature communications*, 7(1):1–7, 2016.
- [32] D Yu Vodolazov, F M Peeters, M Morelle, and V V Moshchalkov. Masking effect of heat dissipation on the current-voltage characteristics of a mesoscopic superconducting sample with leads. *Physical Review B*, 71(18):184502, 2005.
- [33] A V Silhanek, M V Milošević, R B G Kramer, G R Berdiyrov, J Van de Vondel, R F Luccas, T Puig, F M Peeters, and V V Moshchalkov. Formation of stripelike flux patterns obtained by freezing kinematic vortices in a superconducting pb film. *Physical review letters*, 104(1):017001, 2010.
- [34] Ž L Jelić, M V Milošević, J Van de Vondel, and A V Silhanek. Stroboscopic phenomena in superconductors with dynamic pinning landscape. *Scientific reports*, 5:14604, 2015.
- [35] Ž L Jelić, M V Milošević, and A V Silhanek. Velocimetry of superconducting vortices based on stroboscopic resonances. *Scientific reports*, 6:35687, 2016.
- [36] L P Gor’kov and N B Kopnin. Vortex motion and resistivity of type-II superconductors in a magnetic field. *Soviet Physics Uspekhi*, 18(7):496, 1975.
- [37] L Kramer and A Baratoff. Lossless and dissipative current-carrying states in quasi-one-dimensional superconductors. *Physical Review Letters*, 38(9):518, 1977.
- [38] W D Gropp, H G Kaper, G K Leaf, D M Levine, M Palumbo, and V M Vinokur. Numerical simulation of vortex dynamics in type-II superconductors. *Journal of Computational Physics*, 123(2):254–266, 1996.
- [39] M V Milošević and R Geurts. The ginzburg-landau theory in application. *Physica C: Superconductivity*, 470(19):791–795, 2010.
- [40] E Sardella, A L Malvezzi, P N Lisboa-Filho, and W A Ortiz. Temperature-dependent vortex motion in a square mesoscopic superconducting cylinder: Ginzburg-landau calculations. *Physical Review B*, 74(1):014512, 2006.
- [41] D Yu Vodolazov. Effect of surface defects on the first field for vortex entry in type-II superconductors. *Physical Review B*, 62(13):8691, 2000.
- [42] R Tidecks and Th Werner. Continuous change from weak to strong coupling behavior in quasi-one-dimensional superconductors. *Journal of low temperature physics*, 65(3-4):151–184, 1986.
- [43] L P Gorkov and N B Kopnin. Viscous vortex flow in superconductors with paramagnetic impurities. *J. Exp. Theor. Phys.*, 33(6):1251–1256, 1971.
- [44] V V Baranov, A G Balanov, and V V Kabanov. Current-voltage characteristic of narrow superconducting wires: Bifurcation phenomena. *Physical Review B*, 84(9):094527, 2011.
- [45] B I Ivlev, N B Kopnin, and L A Maslova. Dynamics of the resistive state of a superconductor. *Sov. Phys.-JETP*

- (Engl. Transl.);(United States), 51(5), 1980.
- [46] B I Ivlev, N B Kopnin, and I A Larkin. Low-frequency oscillations in the resistive state of narrow superconductors. *Sov. Phys. JETP*, 61(2):337–343, 1985.
- [47] R Zadorosny, E Sardella, A L Malvezzi, P N Lisboa-Filho, and W A Ortiz. Crossover between macroscopic and mesoscopic regimes of vortex interactions in type-II superconductors. *Physical Review B*, 85(21):214511, 2012.
- [48] Xiaofu Zhang, Adriana E. Lita, Mariia Sidorova, Varun B. Verma, Qiang Wang, Sae Woo Nam, Alexei Semenov, and Andreas Schilling. Superconducting fluctuations and characteristic time scales in amorphous WSi. *Phys. Rev. B*, 97:174502, May 2018.
- [49] G. R. Berdiyrov, M. V. Milošević, and F. M. Peeters. Kinematic vortex-antivortex lines in strongly driven superconducting stripes. *Physical Review B*, 79(18), 2009.
- [50] F. Brosens, J.T. Devreese, V.M. Fomin, and V.V. Moshchalkov. Superconductivity in a wedge: analytical variational results. *Solid State Communications*, 111(10):565–569, 1999.
- [51] Mariia V. Sidorova, A. G. Kozorezov, A. V. Semenov, Yu. P. Korneeva, M. Yu. Mikhailov, A. Yu. Devizenko, A. A. Korneev, G. M. Chulkova, and G. N. Goltsman. Nonbolometric bottleneck in electron-phonon relaxation in ultrathin wsi films. *Phys. Rev. B*, 97:184512, May 2018.
- [52] Lu Zhang, Lixing You, Xiaoyan Yang, Yan Tang, Mengting Si, Kaixin Yan, Weijun Zhang, Hao Li, Hui Zhou, Wei Peng, and Zhen Wang. Hotspot relaxation time in disordered niobium nitride films. *Applied Physics Letters*, 115(13):132602, 2019.
- [53] M Yu Kupriyanov and K K Likharev. *ZhETF Pis. Red.*, 15, 1972.
- [54] N Fogel. Temperature dependence of the viscosity coefficient in type II superconductors. *Sov. Phys. JETP*, 36(4):725–730, 1973.
- [55] V N Gubankov. Resistance of thin superconducting films in the dynamic mixed state. Technical report, Institute of Radio Technology and Electronics, Academy of Sciences of the Soviet Union, 1973.
- [56] T Takayama. Flux flow resistivity of superconducting thin film. *Journal of Low Temperature Physics*, 27(3-4):359–396, 1977.
- [57] S J Poon and K M Wong. Viscous flow of vortices in ideal type-II amorphous superconductors. *Physical Review B*, 27(11):6985, 1983.
- [58] D Halbertal, J Cuppens, M B Shalom, L Embon, N Shadmi, Y Anahory, H R Naren, J Sarkar, A Uri, Y Ronen, et al. Nanoscale thermal imaging of dissipation in quantum systems. *Nature*, 539(7629):407–410, 2016.
- [59] M V Milošević, G R Berdiyrov, and F M Peeters. Fluxonic cellular automata. *Applied Physics Letters*, 91(21):212501, 2007.
- [60] M V Milošević and F M Peeters. Vortex manipulation in a superconducting matrix with view on applications. *Applied Physics Letters*, 96(19):192501, 2010.
- [61] T Golod, A Iovan, and V M Krasnov. Single abrikosov vortices as quantized information bits. *Nature communications*, 6(1):1–5, 2015.